1 # Controlling shell-side crystal nucleation in a gas-liquid membrane contactor
2 # for simultaneous ammonium bicarbonate recovery and biogas upgrading

3

4 A. McLeod, P. Buzatu, O. Autin, B. Jefferson and E. McAdam[*]
5 Cranfield Water Science Institute, Building 39, Cranfield University, Bedfordshire, MK43 0AL, UK
6 *Corresponding author e-mail: e.mcadam@cranfield.ac.uk

7

8 **Abstract**

9 A gas-liquid hollow fibre membrane contactor (HFMC) process has been introduced for carbon

10 dioxide (CO_2) separation from biogas where aqueous ammonia (NH_3) is used to chemically enhance

11 CO_2 absorption and initiate heterogeneous nucleation of the reaction product ammonium

12 bicarbonate at the membrane-solvent interface. Aqueous ammonia absorbents (2 to 7 M) were

13 initially used in single pass for CO_2 separation from a synthetic biogas where nucleation of

14 ammonium bicarbonate crystals was observed at the perimeter of the micropores. Recirculation of

15 the aqueous ammonia absorbent encouraged the growth of ammonium bicarbonate crystals on the

16 shell-side of the membrane that measured several microns in diameter. However, at high aqueous

17 NH_3 concentrations (3-7 M), lumen side crystallisation occurred and obstructed gas flow through the

18 lumen of the HFMC. The suggested mechanism for lumen-side crystallisation was absorbent

19 breakthrough into the lumen due to pore wetting which was promoted by low absorbent surface

20 tension at high NH_3 concentration. Preferential shell-side nucleation can therefore be promoted by:

21 (1) raising surface tension of the absorbent; and, (2) selection of a membrane with a more regulated

22 pore shape than the PTFE membrane used (d/L 0.065) as both actions can diminish solvent ingress

23 into the pore. This was evidenced using 2 M NH_3 absorbent where shell-side crystallisation was

24 evidenced without the onset of lumen side crystallisation. Raising surface tension through the

25 inclusion of salt into the chemical absorbent also promoted greater CO_2 flux stability. Importantly,

26 this study demonstrates that chemically enhanced HFMC are an attractive prospect for gas-liquid

27 separation applications where reaction product recovery offers further economic value.

28

29 *Keywords:*   biomethane, membrane crystalliser, chemical absorption, crystallisation

30 **1.   Introduction**

31 Many water utilities are now refining biogas into biomethane rather than using directly for electrical

32 production due to the potential for higher revenue. To illustrate, in the UK, through support under

33 the Renewable Heat Incentive (RHI), the revenue expected from biomethane is €0.39 m^{-3} which

34 compares to only €0.23 m^{-3} for electrical production (Read et al., 2010). The biomethane product

35 must achieve methane quality that is equivalent or higher than natural gas (>81%) which therefore

36 demands the separation of carbon dioxide (CO_2) from biogas. This is generally facilitated using

37 absorption in a packed column and is analogous to those currently trialled for carbon capture and

38 storage (CCS). In CCS applications, process intensification is provided through the inclusion of a

39 chemical solvent (e.g. monoethanolamine) that reacts with CO_2 to enhance the separation.

40 However, the energy demanded for chemical solvent regeneration, coupled with solvent losses (due

41 to volatility and degradation pathways) and the demand for specialist operators has limited uptake

42 of chemical absorption for biogas upgrading by water utilities (Heile et al., 2014).

43   Ammonia is now recognised as an emerging chemical absorbent in CCS due to its higher

44 absorption efficiency, greater chemical stability and lower energy demand for regeneration

45 (Shuangchen et al., 2013; Makhloufi et al., 2014). Aqueous ammonia (NH_3) absorption therefore

46 presents comparable advantages for water utilities undertaking biogas upgrading, but also offers the

47 unique opportunity to utilise the ammonia rich wastewater produced onsite as a low cost absorbent

48 feedstock for enhanced CO_2 separation. The reaction between free NH_3 and CO_2 is known to proceed

49 by (Eq. 1) where ammonium bicarbonate (NH_4HCO_3) is the reaction product formed:

50 $$CO_2 + NH_3 + H_2O \rightarrow \left(NH_4\right)HCO_3 \qquad\qquad (1)$$

51 When recovered in crystalline form, NH_4HCO_3 can be used as an ammonia rich fertiliser as well as a

52 feedstock in commercial manufacture. Consequently, controlled production of a crystalline NH_4HCO_3

53 reaction product from ammonia rich wastewaters posits several advantages for biogas upgrading at

54 sewage works including: further reduction in energy demand for absorbent regeneration; a

55   reduction in load onto nitrification/denitrification processes (€3 kgN^{-1}); and, production of NH$_4$HCO$_3$

56   as a new revenue stream (bulk cost €111 tonne^{-1}) (Thornton, 2007).

57   To enable recovery of crystalline products within a controlled environment, Curcio et al.

58   (2001) introduced the membrane crystallisation reactor (MCr). In their work, a microporous

59   hydrophobic membrane contactor (HFMC) was used to facilitate non-dispersive contact between a

60   heated undersaturated crystallising solution (on the retentate side) and cooled pure water on the

61   permeate side. The temperature differential provided the gradient for vapour transport from the

62   crystallising solution through the membrane pores enabling an increased solute concentration

63   (sodium chloride, NaCl) which upon exceeding its solubility limit, initiated nucleation and growth of

64   NaCl crystals (Figure 1). The underpinning mechanism by which the MCr operates therefore

65   corresponds to evaporation-migration-condensation (Di Profio et al., 2010) and has been used to

66   recover NaCl and magnesium sulfate from nanofiltration retentate as crystalline products (Drioli et

67   al., 2004) and for the controlled production of Lysozyme crystals (Di Profio et al., 2003).

68   The same microporous HFMC technology used to control crystallisation in MCr systems has

69   now also been used to enable CO$_2$ separation from biogas through supporting an analogous

70   absorption mechanism to conventional absorption columns (Heile et al., 2014). In this case, the

71   hydrophobic membrane facilitates non-dispersive contact between the chemical absorbent and gas

72   phase with the gases free to diffuse through the open pore structure. Due to the increase in specific

73   surface area afforded by the membrane contactor, the technology presents an inherent advantage

74   in reducing both process scale and absorption solvent consumption, relative to conventional

75   columns (Herzog and Pederson, 2000). In this study, we therefore seek to introduce a gas-liquid

76   membrane absorption crystallisation reactor that enables both the selective separation of CO$_2$

77   through reaction with ammonia and the subsequent nucleation and growth of the crystalline

78   ammonium bicarbonate reaction product for recovery. The mechanism for nucleation and growth of

79   NH$_4$HCO$_3$ crystals in this study differs from classical MCr systems in that supersaturation is achieved

80   by counter diffusion of solutes through the transport of CO$_2$ molecules from the gas phase into the

81 crystallising fluid (an aqueous ammonia absorbent) where the driving force for CO_2 transport to the

82 crystallising fluid is the enhancement in solubility provided by the chemical reaction with NH_3.

83 Nucleation is then dependent upon CO_2 reaching sufficient concentration to initiate local

84 supersaturation of the solvent (Figure 1).

85 Makhloufi et al. (2014) recently screened a number of hollow-fibre membrane materials to

86 determine compatibility for CO_2 absorption into aqueous ammonia for chemically enhanced post

87 combustion CCS. The authors remit precluded an interest in recovering NH_4HCO_3 as a byproduct and

88 determined that microporous fibres were inappropriate for application to CCS due to CO_2 flux

89 instability caused by ammonium bicarbonate precipitation on the gas-side (lumen-side) of the

90 membrane. In this study, we therefore seek to introduce the mechanism underpinning controlled

91 nucleation and growth of ammonium bicarbonate on the shell-side (absorbent side) of a

92 microporous HFMC to illustrate the potential of the gas-liquid membrane absorption crystallisation

93 reactor for simultaneous gas separation with reaction product recovery. A microporous

94 polytetrafluoroethylene (PTFE) HFMC is therefore used to investigate: (i) the potential for chemical

95 absorption in a microporous membrane to enable shell-side (absorbent side) crystal nucleation; (ii)

96 investigation of absorbent conditions required to enable crystal growth; and (iii) the role of the

97 microporous substrate in controlling nucleation. To our knowledge, this is the first study to describe

98 the use of hydrophobic microporous membranes for the controlled nucleation and growth of a

99 reactant product following chemical absorption from the gas phase.

100

101 **2.   Experimental**

102 *2.1   Fabrication, setup and operation of equipment*

103 Hydrophobic micro-porous PTFE fibres obtained from Markel Corporation (Plymouth Meeting,

104 Pennsylvania, USA) and comprised a 200 μm wall thickness and 44% porosity (Table 1). To enable

105 characterisation of crystal growth with minimal disturbance, single fibre modules were

106 manufactured. Modules comprised a transparent PVC shell with an inner diameter of 0.004 m and

107   were completed with two acetal push-fit T-union-joints (1/4" Speedfit, John Guest Ltd., Middlesex,

108   UK). Fibres were potted in epoxy resin (Bostik Ltd., Stafford, UK). For dense membrane experiments,

109   polydimethylsiloxane (PDMS) fibres with a wall thickness of 65 μm were used in an identical module

110   construction (Trelleborg sealing solutions, Stuttgart, Germany).

111   Methane (CH_4, 99.995%) and carbon dioxide (CO_2, 99.7%) (BOC gases, Ipswich, UK) were

112   mixed in controlled proportions using mass flow controllers (0.2-20.0 l min^{-1}, Roxspur Measurement

113   and Control Ltd., Sheffield, UK) to provide an initial 50:50 CH_4:CO_2 gas composition and introduced

114   through the fibre lumen (Figure 2). Liquid was pumped co-currently into the shell-side.

115   Transmembrane pressure (TMP) was monitored by digital pressure gauges (DPG1000, Omega

116   Engineering Ltd., Manchester, UK) and liquid and pressure flow controlled using needle valves.

117

118   *2.2   Sampling and analyses*

119   Ammonia absorbents were prepared through dilution of an NH_3 concentrate (35 %, Fisher

120   Chemicals, Loughborough, UK) using de-ionised (DI) water (15.0 MΩ cm^{-1}). Absorbent pH was fixed

121   to pH 11 to ensure 100% of the ammoniacal nitrogen was available as un-ionised free NH_3 (Thurston

122   et al., 1979). Ammonia concentrations were confirmed by use of an ammonium cell test (4-80 mg l^{-1},

123   VWR International Ltd., Poole, UK) with subsequent determination by spectrophotometry

124   (Spectroquant Nova 60, Merck-Millipore, Darnstadt, Germany). Gas composition was determined

125   using an infrared biogas analyser sited on the gas outlet (range 0-100 %, accuracy <0.2 % full-scale;

126   Yieldmaster, Bluesens gas sensor GmbH, Herten, Germany). Subsequently, CO_2 removal efficiency

127   was determined based upon the binary gas composition before and after the membrane module:

128    $CO_2 \ removal \ efficiency \ (\%) = \frac{(c_{G,in} - c_{G,out})}{c_{G,in}} \times 100$ (2)

129   where $c_{G, \ in}$ and $c_{G, \ out}$ are gas phase CO_2 concentrations before and after the HFMC respectively (mol

130   mol^{-1}). Gas flow rate exiting the contactor was measured using a bubble flow meter (50 ml, Restek,

131   Bellefonte, US) and used to calculate carbon dioxide flux (J_{CO2}, mol m^{-2} s^{-1}):

132 $$J_{CO_2} = \frac{[(Q_{G,in} \times c_{G,in}) - (Q_{G,out} \times c_{G,out})] \times 273.15 \times 1000}{(22.4 \times A_m \times T_G)}$$ (3)

133 where $Q_{G,\ in}$ and $Q_{G,\ out}$ are gas flow rate before and after HFMC respectively (m^3 s^{-1}), A_m is the

134 membrane surface area for absorption (m^2) and T_G is the gas temperature (K) (Atchariyawut et al.,

135 2007).

136　　　　Examination of the PTFE microporous membrane pore structure was determined using a

137 scanning electron microscope (SEM) equipped with a field emission gun (sFEG) (XL30, FEI, Hillsboro,

138 Oregon, USA). Pores size data was subsequently analysed to provide a size distribution using a log-

139 normal distribution function (Li et al., 2000):

140 $$f_L(r) = \frac{1}{\sqrt{2\pi r}} [ln(1 + \sigma^2)]^{-0.5} \times exp\left[-\frac{\left(ln(r/r_m)(1+\sigma^2)^{0.5}\right)^2}{2 \times ln(1+\sigma^2)}\right]$$ (4)

141 Surface roughness of the virgin fibres was characterised using atomic force microscopy (AFM,

142 Dimension 3100, Bruker, Massachusetts, US). Examination of sacrificial membrane samples to

143 determine crystal nucleation and growth was conducted using SEM (upto x10000 magnification) for

144 the finer diameter PTFE fibres, and optical microscope for the wider diameter PDMS fibres. Fibre

145 samples for SEM were first coated with gold-palladium (Au-Pd) using a cool sputtering SEM coating

146 unit (E5100, Polaron Equipment/Quorum Technologies Ltd., Lewes, UK). Spectroscopic elemental

147 analysis was performed in tandem with SEM by energy dispersive x-ray spectroscopy (EDX) using

148 Aztec software (Oxford Instruments NTS, Abingdon, UK). Solvent surface tension was determined

149 using a Du Noüy ring tensiometer (Kruss K6, Bristol, UK).

150

151 **3.　　　Results**

152 *3.1　　Characterisation of the PTFE and PDMS membranes*

153 Pore size analysis by SEM indicated that average pore radius of the PTFE fibres was 0.157 μm with

154 radii distributed within a range between 0.13 μm and 0.21 μm (Figure 3). This closely approximates

155 to pore width data provided by the manufacturer (Table 1). The stretched length of the pores was

156 approximately 4.9±3.1 μm, yielding a pore diameter to length ratio (*d/L*) of 0.065. Average surface

157 roughness of the PTFE fibres was 82 nm which is similar to that measured for the nonporous PDMS

158 membrane (77 nm).

159

160 *3.2 Removal of CO_2 using NH_3 as a chemical absorbent*

161 The PTFE HFMC was initially tested in single pass mode (without absorbent recirculation). Gas

162 velocity, V_G, was varied between 0.28 m s^{-1} and 18.62 m s^{-1} whilst both liquid velocity (V_L) and

163 aqueous ammonia absorbent concentration were fixed at 0.02 m s^{-1} and 7 mol l^{-1} respectively (Figure

164 4). Maximum CO_2 removal efficiency of 72 % was observed at the lowest V_G examined which

165 corresponded to a G/L ratio of 3. For these fixed conditions, methane content increased from 50% at

166 the inlet to 86% CH_4. As V_G was increased, CO_2 removal efficiency decreased to a minimum of 3.6%

167 which was recorded at the highest V_G tested (18.62 m s^{-1}). Whilst CO_2 removal efficiency declined

168 with an increase in V_G, CO_2 flux increased from 0.015 to 0.116 mol m^{-2} s^{-1} within the gas velocity

169 range tested (Figure 4). Microscopic analysis of the shell-side of a PTFE fibre that had been used with

170 7 mol l^{-1} aqueous ammonia solution and a G/L ratio of 10, showed white specks formed around the

171 pore mouths indicating that crystal nucleation had been initiated (Figure 5).

172

173 *3.3   Identification of heterogeneous crystal growth*

174 Crystal growth on the shell side of the module was identified within each of the 2 to 5 M NH_3

175 absorbents used (V_G = 0.93 m s^{-1}, G/L 10) with carbon (C), oxygen (O) and nitrogen (N) peaks

176 confirmed in the crystals formed by EDX (Table 2). Crystals that had grown in 3 to 5 molNH_3 l^{-1}

177 absorbents generally developed planar structures that were oriented roughly parallel to the

178 membrane surface with multiple points of contact, whereas those formed in the 2 molNH_3 l^{-1}

179 absorbent developed perpendicular to the membrane surface with fewer crystal-membrane contact

180 points. Following two to five absorbent recirculations (five second residence time per recirculation in

181 the PTFE HFMC), a progressive decline in CO_2 flux was observed at each free ammonia concentration

182 tested (Figure 6). After 6 and 13 recirculations respectively (30 s to 65 s), the 3 and 5 mol l^{-1} NH_3

183   absorbent experiments were stopped due to lumen-side crystallisation which blocked the flow of gas

184   (Figure 7). Lumen side crystals were tightly packed and propagated along the length of the hollow

185   fibre. A similar progressive decline in CO_2 flux was also observed using 2 $molNH_3\ l^{-1}$ absorbent.

186   However, whilst shell-side crystallisation was evidenced in the 2 $molNH_3\ l^{-1}$ absorbent (Table 2),

187   lumen-side crystallisation was not observed following 34 absorbent recirculations (170 s).

188

189   *3.4   Using membrane type to control lumen-side crystallisation*

190   Performance of a nonporous PDMS membrane (Figure 8) was compared to the microporous

191   membrane performance by recirculating 5 $molNH_3\ l^{-1}$ absorbent and fixing hydrodynamic conditions

192   sufficient to yield equivalent CO_2 fluxes to the PTFE membrane (G/L 0.39, Figure 8). Under these

193   conditions the NH_3 solvent had a 1 s residence time within the PDMS HFMC. A steady state period

194   was observed between 400 and 800 solvent recirculations, which corresponded to CO_2 fluxes of

195   around 0.014 mol $m^{-2}\ s^{-1}$. However, after around 800 recirculations a progressive decline in CO_2 flux

196   was noted and the experiment was terminated after 931 recirculations. Whilst crystals were

197   observed to have grown on the shell-side of the PDMS fibre (Figure 9), the reduction in CO_2 flux after

198   800 recirculations coincided with the formation of crystalline solid within the fibre lumen inducing

199   deformation of the cylindrical fibre structure.

200

201   *3.5   Manipulating solvent chemistry to promote shell-side nucleation on PTFE fibres*

202   Carbon dioxide flux provided by the PTFE membrane using 3 $molNH_3\ l^{-1}$ absorbent during

203   recirculation were compared when using 1% wt. glycerol as an additive to the 3 $molNH_3\ l^{-1}$ absorbent

204   as the addition of glycerol has been shown to diminish the volatility of ammonia (Shuangchen et al.,

205   2013)(Figure 10). With the glycerol added, initial mean CO_2 flux was 3.5 % lower than without

206   glycerol addition and after 12 recirculations, CO_2 flux was 23 % lower than with the pure 3 $molNH_3\ l^{-1}$

207   absorbent. Conversely, the addition of 5% wt. NaCl to the 3 $molNH_3\ l^{-1}$ absorbent increased CO_2 flux

208   stability. To illustrate, after 13 recirculations of the 3 $molNH_3$ l^{-1} absorbent with 5% wt. NaCl added,

209   CO_2 flux was 91% of initial flux in comparison to only 81% for the 3 $molNH_3$ l^{-1} absorbent.

210   The change in surface tension following an increase in NaCl or aqueous ammonia

211   concentration to deionised water was studied (Figure 11). With the inclusion of between 0.1 and 1

212   M NaCl (5.85% wt.), surface tension increased by up to 2.2 mN m^{-1}. However, a reduction in surface

213   tension of between -0.8 and -8.7 mN m^{-1} was measured for concentrations between 0.3 and 7

214    $molNH_3$ l^{-1} which is within the range of aqueous ammonia absorbents studied and is consistent with

215   the literature (Weissenborn et al., 1995). The addition of 5% wt. NaCl to aqueous ammonia reduced

216   the change in surface tension. For example, at a concentration of 3 $molNH_3$ l^{-1} a reduction in surface

217   tension of -6.7 mN m^{-1} was recorded whereas with the inclusion of 5% wt. NaCl, the change in

218   surface tension reduced to only -3.9 mN m^{-1}.

219

220   **4. Discussion**

221   In this study, the use of a liquid phase chemical reaction to enhance CO_2 absorption and produce a

222   crystalline reaction product has been demonstrated using a PTFE microporous hydrophobic hollow

223   fibre membrane to promote the nucleation and growth of ammonium bicarbonate. During single

224   pass experiments using a 7 mol l^{-1} ammonia absorbent, an increase in V_G increased CO_2 flux into the

225   receiving ammonia absorbent. In chemically reactive absorption systems, an increased gas phase

226   flow rate is often observed to mediate solute flux (Esquiroz-Molina et al., 2013) as this enables

227   replenishment of CO_2 at the solvent-membrane interface and maintenance of a high bulk gas CO_2

228   partial pressure (Zeng et al., 2013). When operating at high V_G (G/L 10) using 7 mol l^{-1} ammonia

229   absorbent (CO_2 flux 0.116 mol m^{-2} s^{-1}, Figure 4), an absorption rate of 44.2 kmol m^{-3} h^{-1} was recorded

230   ($kmolCO_2$ m^{-3} absorption reactor volume h^{-1}). For comparison, Zeng et al. (2013) recorded a CO_2

231   absorption rate of 3.3 kmol m^{-3} h^{-1} in a packed column using aqueous ammonia (4.5 mol l^{-1}), which

232   illustrates the high rate of CO_2 transfer achieved with the micro-porous HFMC. For this high flux

233   condition, activation of a substantial number of nucleation sites around the micro-pores on the

234   shell-side of the PTFE was demonstrated (Figure 5). This is supported by the work of Di Profio et al.

235   (2003) where increased solute concentration enhanced supersaturation leading to an excess of

236   nucleation. Interestingly, crystallisation is generally not observed in CO_2 /aqueous ammonia packed

237   columns unless the ammonia concentration exceeds around 6 mol l^{-1} (Budzianowski et al., 2011). In

238   this study, nucleation and crystal growth was observed at 2 mol l^{-1} (Table 2). The enhanced

239   nucleation potential of the hydrophobic PTFE membrane can be explained by the high contact angle

240   exhibited (around 129° for PTFE-water: Guillen-Burrieza et al., 2013; Zhu et al., 2013) which favours

241   heterogeneous nucleation over homogeneous nucleation (Figure 12). The contact angle reflects the

242   three phase line at the perimeter of the pore mouth, where the CO_2 gas phase, aqueous ammonia

243   phase and PTFE solid phase interact (Figure 1; Curcio et al., 2006) and accounts for the proximity of

244   nucleation sites relative to the pore mouth. The inclusion of pores reduces the thermodynamic

245   preference for heterogeneous nucleation, although this is compensated for by the selection of a

246   more hydrophobic material. Additionally, the provision of specific sites for nucleation at three phase

247   line around the pore mouths, materials with increased porosity show an enhanced rate of

248   nucleation, offering a kinetic preference for nucleation upon the membrane that complements the

249   stability due to high contact angle (Curcio et al., 2006). It is proposed that the nucleation mechanism

250   is analogous to that underpinning evaporation-migration-condensation as seen in MCr which is

251   thought to follow: (1) surface adsorption through non-specific attractive interaction; (2) hindrance of

252   lateral migration by the irregular pore structure causing packing; and (3) molecular entrapment

253   which induces relatively higher supersaturation (Di Profio et al., 2010). However, within the gas

254   crystallisation process proposed, CO_2 will migrate from the gas phase through the stagnant region of

255   the solvent meniscus resident within the pore to the nucleation site, the rate of which will be

256   determined by the reactivity of the solvent.

257   Growth of ammonium bicarbonate crystals on the shell-side of the membrane was

258   demonstrated following recirculation of the ammonia absorbent (Table 2). Crystals grown within 3

259   and 5 molNH_3 l^{-1} absorbents differed from those grown within 2 molNH_3 l^{-1} absorbent which were

260 characterised by growth perpendicular to the membrane surface and from a comparatively limited

261 number of nucleation points. Lowering the aqueous ammonia concentration to 2 molNH$_3$ l^{-1} results

262 in two effects: (1) this is close to the nominal limiting saturation concentration for the reactant

263 product (NH$_4$HCO$_3$, 2.24 mol l^{-1}); and (2) the flux of CO$_2$ into the aqueous phase is reduced due to the

264 lower absorbent reactivity. The crystal orientation identified at low fluxes is indicative of conditions

265 favouring crystal growth over nucleation, and is analogous to observations made previously when

266 employing low solvent fluxes for evaporative MCr (Zhang et al., 2008) which results in production of

267 fewer larger crystals. Controlling preference for the growth of fewer, larger crystals perpendicular to

268 the membrane surface may be key to harvesting of the NH$_4$HCO$_3$ product, where it has been

269 indicated that shear stresses due to axial liquid flow are sufficient to detach crystals grown upon the

270 hydrophobic surface (Di Profio et al., 2010).

271 Following extensive solvent recirculation, crystal growth was observed on the lumen side of

272 the PTFE fibre (Figure 7). In a preliminary evaluation of CO$_2$ absorption into aqueous NH$_3$ using

273 oxyphan® microporous hollow fibres, Makhloufi et al. (2014) postulated that the CO$_2$ flux decline

274 observed was due to lumen-side (gas-side) crystallisation which initiated through high ammonia slip

275 into the humidified gas phase. To investigate this mechanism, in this study, glycerol (1%) was added

276 to the aqueous ammonia absorbent used with the microporous PTFE membranes as this is

277 commonly employed to suppress NH$_3$ volatility by the glycerol hydroxyl group bonding to the free

278 ammonia (Shuangchen et al., 2013). However, with the inclusion of glycerol, CO$_2$ flux declined more

279 rapidly than without glycerol addition suggesting that glycerol-ammonia bonding also retarded mass

280 transfer (Cheng et al., 2003). Direct measurement of ammonia slip could not be made in this study

281 due to scale. However, ammonia slip has been measured by this group using a larger contactor scale

282 (0.79 m^2) and similar process conditions (5 mol l^{-1} aq. NH$_3$; G/L 7.5) and a slip of only 0.015 % NH$_3$

283 noted which is ostensibly insufficient to grow the crystal mass observed within the fibre. The low slip

284 can be explained by the low liquid velocities imposed, for which the depletion of ammonia through

285 reaction with CO$_2$ extends radially away from the fibre wall toward the bulk (Figure 13). This is

286 experimentally corroborated at high G/L ratios where high CO_2 fluxes are coincident with diminished

287 CO_2 removal efficiency (Figure 4) due to the decrease in mole ratio between NH_3 and CO_2 in the

288 reaction zone (Zeng et al., 2013). At a G/L of 3, the methane content in the outlet gas exceeding the

289 CH_4 content of North Sea natural gas (Persson et al., 2007) which indicated that the gas treatment

290 objective can be met whilst limiting the free ammonia concentration (and hence slip) at the gas-

291 liquid interface.

292   Higher aqueous ammonia concentrations were demonstrated to lower absorbent surface

293 tension considerably (Figure 11). Lower surface tension is known to decrease breakthrough pressure

294 for a cylindrical pore (Franken et al., 1987) which notably enhances the probability for wetting:

295
$$\Delta P_{B.P.} = \frac{-4B\sigma\cos\theta}{d_{max}} \tag{5}$$

296 It is suggested that the reduction in surface tension observed at high aqueous ammonia

297 concentration enables penetration of the ammonia rich absorbent into the pore and into the CO_2

298 rich gas phase initiating crystal nucleation in the lumen side of the microporous membrane. This was

299 evidenced by the faster onset of lumen-side (gas-phase) crystal growth within aqueous ammonia

300 concentrations greater than 3 M, which were characterised by a relatively large reduction in surface

301 tension ($\Delta\sigma$ -5.6 to -9.6 mN m^{-1}, Figure 11). For comparison, whilst shell-side crystallisation was

302 noted within the lower concentration 2 molNH$_3$ l^{-1} absorbent, lumen-side crystal growth was absent.

303 However, the progressive and gradual decline in CO_2 flux noted for the 2 molNH$_3$ l^{-1} absorbent

304 remains indicative of progressive pore wetting (Bougie et al., 2013); it is therefore asserted that the

305 lower surface tension change measured at 2 molNH$_3$ l^{-1} was insufficient to enable complete

306 breakthrough into the lumen side. The role of surface tension in inhibiting both lumen-side

307 crystallisation and wetting was confirmed through the addition of 5% wt. sodium chloride which

308 counteracted the transition in surface tension introduced by the aqueous ammonia. Whilst the

309 inclusion of NaCl increased surface tension of the aqueous ammonia by only 2.8 mN m^{-1}, a marked

310 increase in CO_2 flux stability was observed (Figure 10, Figure 11).

311   Dense PDMS hollow fibre membranes were also evaluated as an approach to diminish lumen

312 side crystallisation observed with microporous membranes at high aqueous concentrations, as they

313 increase resistance to absorbent breakthrough whilst also being hydrophobic (contact angle with

314 water approximately 110°: Aerts et al., 2006; Jadav et al., 2012). Whilst some crystal growth was

315 observed on the shell-side of the PDMS membrane, crystal growth predominated on the lumen-side

316 of the membrane within the gas phase (Figure 9). To generate analogous flux rates to those of the

317 PTFE membrane, a high liquid velocity was used (G/L 0.39) which enhances surface renewal of free

318 ammonia at the absorbent-membrane boundary and hence the potential for ammonia slip.

319 Furthermore, since ammonia is a smaller and more condensable molecule than CO_2, it is more

320 permeable through PDMS (Makhloufi et al., 2014). Consequently co-permeability of both free

321 ammonia and water vapour in the dense PDMS membrane promoted crystal growth within the fibre

322 lumen and within the dynamic free volume network of the rubbery PDMS membrane which induced

323 fibre wall distortion. Wetting and subsequent lumen-side crystallisation can be ascribed to the

324 stretched pore shape of the microporous membrane in this study in addition to the surface tension

325 of the absorbent. Stretched pores are a common feature of several commercially available

326 hydrophobic polymeric microporous membranes (*d/L* 0.48, Heile et al., 2014) but was exacerbated

327 within the PTFE fibre studied (*d/L* 0.065). Franken et al. (1987) introduced a pore geometry

328 coefficient (*B*) to the Laplace-Young equation (Eq. 5) where non-cylindrical pore shape was classified

329 by a coefficient of between 0<*B*<1. This emphasises that pore wetting in exacerbated as pore shape

330 tends away from that of a cylinder (Bougie et al., 2013). Consequently, microporous membranes

331 with tighter pore shape together with surface tension regulation of the solvent are recommended to

332 encourage preferential shell-side crystallisation and enhanced CO_2 flux stability in gas-liquid

333 membrane absorption crystallisation reactors.

334

335 **5. Conclusions**

336   The use of microporous hollow fibre membrane contactors has been introduced to enable the

337   nucleation and growth of crystalline reaction products initiated through chemically facilitated CO_2

338   separation from the gas phase. This represents the first membrane crystallisation reactor where the

339   solubility limit to initiate nucleation is reached through counter diffusion of solutes from the solvent

340   bulk to the membrane and of solutes from the 'permeate-side' through the membrane micropores

341   into the membrane-solvent boundary. Lumen-side crystallisation can be avoided in favour of

342   preferential shell-side nucleation and more stable CO_2 fluxes by: (1) raising surface tension of the

343   absorbent through either limiting aqueous ammonia concentration or addition of a surface tension

344   regulator; and, (2) selection of a membrane with a more regulated pore shape than the PTFE

345   membrane used (*d/L* 0.065) as both actions can diminish solvent ingress into the pore. Although

346   limiting aqueous ammonia concentration will diminish solvent reactivity and CO_2 flux, which

347   suggests a larger process scale, the value ascribed to controlled production of the reaction product

348   must also be weighted. Further refinement is required to ensure that longer term CO_2 flux stability

349   can be ascertained simultaneously with ammonium bicarbonate growth. However, the progressive

350   decline in CO_2 flux with the lower ammonia absorbent concentration was notably a result of wetting

351   rather than interference of shell-side crystal growth. Whilst a high initial aqueous ammonia

352   concentration initiated a large number of nucleation sites, the absorbent ammonia concentration

353   also influenced morphology of crystals formed on the shell-side. Crystals formed within lower

354   absorbent ammonia concentration (and lower CO_2 fluxes) possessed fewer nucleation sites and are

355   characteristic of crystals preferentially grown under low flux conditions to favour growth over

356   nucleation. This represents a potentially favourable characteristic for the continued detachment

357   (and hence recovery) of the ammonium bicarbonate crystals formed, where the low shear stresses

358   applied in continuous MCr have been shown sufficient to enable detachment and downstream

359   recovery of the crystalline product (Di Profio et al., 2010).

360

361   **Acknowledgments**

366

367   **References**

368   S. Aerts, A. Vanhulsel, A. Buekenhoudt, H. Weyten, S. Kuypers, H. Chen, M. Bryjak, L.E.M. Gevers,

369   I.F.J. Vankelecom, P.A. Jacobs, Plasma-treated PDMS-membranes in solvent resistant

370   nanofiltration: Characterization and study of transport mechanism, J. Membr. Sci. 275 (2006)

371   212-219.

372   S. Atchariyawut, R. Jiraratananon, R. Wang, Separation of CO_2 from CH_4 by using gas-liquid

373   membrane contacting process, J. Membr. Sci. 304 (2007) 163-172.

374   F. Bougie, M.C. Lliuta, Analysis of Laplace-Young equation parameters and their influence on

375   efficient CO_2 capture in membrane contactors, Sep. Purif. Technol. 118 (2013) 806-815.

376   W.M. Budzianowski, Mitigating NH_3 vaporisation from an aqueous ammonia process for CO_2

377   capture, Int. J. Chem. React. Eng. 9 (2011) 1-27.

378   W.L. Cheng, Z.S. Chen, A. Akisawa, P. Hu, T. Kashiwangi, Theoretical and experimental study on

379   surface tension and dynamic surface tension of aqueous lithium bromide and water with

380   additive, Sci. China 46 (2003) 191-203.

381   E. Curcio, A. Criscuoli, E. Drioli, Membrane crystallizers, Ind. Eng. Chem. Res. 40 (2001) 2679-2684.

382   E. Curcio, E. Fontananova, G. Di Profio, E. Drioli, Influence of the structural properties of

383   poly(vinylidene fluoride) membranes on the heterogeneous nucleation rate of protein

384   crystals, J. Phys. Chem. B 110 (2006) 12438-12445.

385   P.W.J. Derks, G.F. Versteeg, Kinetics of absorption of carbon dioxide in aqueous ammonia solutions,

386   Energ. Proc. 1 (2009) 1139-1146.

387   G. Di Profio, E. Curcio, E. Drioli, Supersaturation control and heterogeneous nucleation in membrane

388   crystallizers: Facts and perspectives, Ind. Eng. Chem. Res. 49 (2010) 11878-11889.

389   G. Di Profio, E. Curcio, A. Cassetta, D. Lambda, E. Drioli, Membrane crystallisation of lysozyme:

390   kinetic aspects, J. Cryst. Growth 257 (2003) 359-369.

391   A. Esquiroz-Molina, S. Georgaki, R. Stuetz, B. Jefferson, E.J. McAdam, Influence of pH on gas phase

392   controlled mass transfer in a membrane contactor for hydrogen sulphide absorption, J.

393   Membr. Sci. 427 (2013) 276-282.

394   M.J.W. Frank, J.A.M Kuipers, W.P.M. Van Swaaij, Diffusion coefficients and viscosities of $CO_2 + H_2O$,

395          $CO_2 + CH_3OH$, $NH_3 + H_2O$, and $NH_3 + CH_3OH$ liquid mixtures, J. Chem. Eng. Data 41 (1996) 297-

396   302.

397   A.C.M. Franken, J.A.M. Nolten, M.H.V. Mulder, D. Bargeman, C.A. Smolders, Wetting criteria for the

398   applicability of membrane distillation, J. Membr. Sci. 33 (1987) 315-328.

399   E. Guillen-Burrieza, R. Thomas, B. Mansoor, D. Johnson, N. Hilal, H. Arafat, Effect of dry-out on the

400   fouling of PVDF and PTFE membranes under conditions simulating intermittent seawater

401   membrane distillation (SWMD), J. Membr. Sci. 438 (2013) 126-139.

402   S. Heile, S. Rosenberger, A. Parker, B. Jefferson, E.J. McAdam, Establishing the suitability of

403   symmetric ultrathin wall polydimethylsiloxane hollow-fibre membrane contactors for

404   enhanced CO2 separation during biogas upgrading, J. Membr. Sci. 452 (2014) 37-45.

405   H. Herzog, O. Falk-Pedersen, The kvaerner membrane contactor: lessons from a case study in how to

406   reduce capture costs. In: Proceedings of the 5th International Conference on Greenhouse Gas

407   Control Technologies, Cairns, August 13–16, 2000.

408   G.L. Jadav, V.K. Aswal, H. Bhatt, J. C. Chaudhari, P. S. Singh, Influence of film thickness on the

409   structure and properties of PDMS membrane, J. Membr. Sci. 415-416 (2012) 624-634.

410   K. Li, J. Kong, X. Tan, Design of hollow fibre membrane modules for soluble gas removal, Chem. Eng.

411   Sci. 55 (2000) 5579-5588.

C. Makhloufi, E. Lasseugette, J.C. Remigy, B. Belaissaoui, D. Roizard, E. Favre, Ammonia based CO_2 capture process using hollow fiber membrane contactors, J. Membr. Sci. 455 (2014) 236-246.

M. Persson, O. Jonsson, A. Wellinger, Biogas upgrading to vehicle fuel standards and grid injection, IEA Bioenergy Task 37 (2007) 20-21.

A. Read, F. Hofmann, Does biogas scrub up? Materials recycling world, December (2011) 20-21.

M. Shuangchen, S. Huihui, Z. Bin, C. Gongda, Experimental study on additives inhibiting ammonia escape in carbon capture process using ammonia method, Chem. Eng. Res. Des. 91 (2013) 2775-2781.

A. Thornton, Application of ion exchange for ammonium removal from municipal wastewaters, PhD Thesis, Cranfield University, 2007.

R.V. Thurston, R. C., Russo, K. Emerson, Aqueous ammonia equilibrium – tabulation of percent un-ionised ammonia, *United States Environmental Protection Agency,* EPA-600 3 (1979) 091.

R. Wang, D.F. Li, D.T. Liang, Modeling of CO_2 capture by three typical amine solutions in hollow fiber membrane contactors, Chem. Eng. Process. 43 (2004) 849-856.

P.K. Weissenborn, R.J. Pugh, Surface tension and bubble coalescence phenomena of aqueous solutions of electrolytes, *Langmuir,* 11 (1995) 1422-1426.

Q. Zeng, Y. Guo, Z. Niu, W. Lin, Mass transfer coefficients for CO_2 absorption into aqueous ammonia solution using a packed column, Ind. Eng. Chem. Res. 50 (2011) 10168-10175.

Q. Zeng, Y., Guo, Z. Niu, W. Lin, The absorption rate of CO_2 by aqueous ammonia in a packed column, Fuel Process. Technol. 108 (2013) 76-81.

X. Zhang, P. Zhang, K. Wei, Y. Wang, R. Ma, The study of continuous membrane crystallisation on lysozyme. Desalination 219 (2008) 101-117.

H. Zhu, H. Wang, F. Wang, Y. Guo, H. Zhang, J. Chen, Preparation and properties of PTFE hollow fiber membranes for desalination through vacuum membrane distillation, J. Membr. Sci. 446 (2013) 145-153.
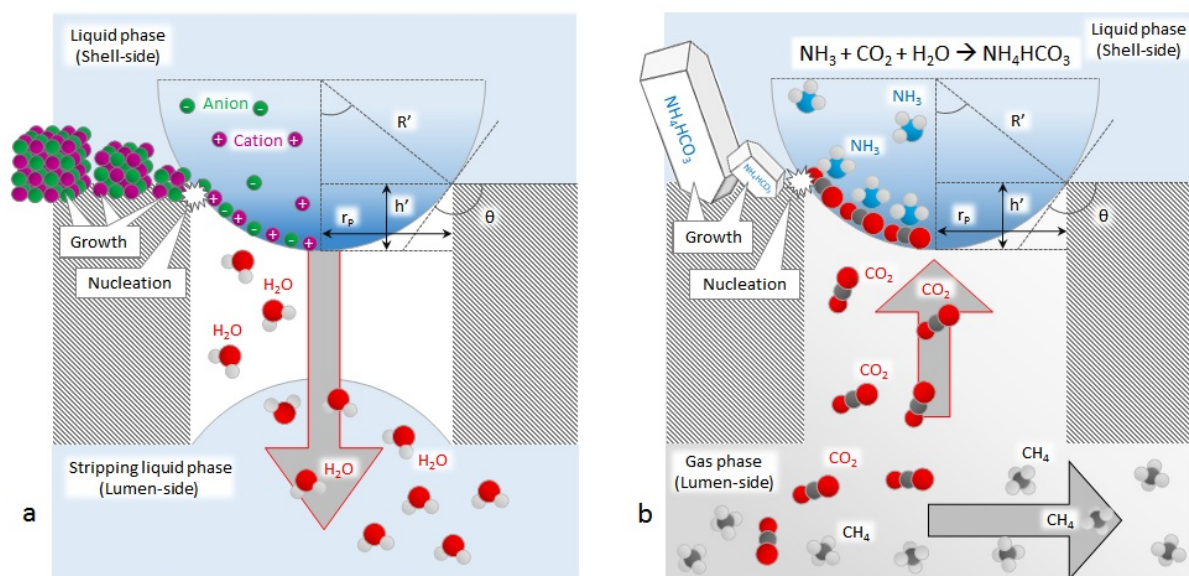
Figure 1. Mechanisms of crystallisation introduced: (a) membrane crystallisers typically achieve supersaturation through removing solvent (often water) as vapour to induce heterogeneous nucleation; and (b) the proposed gas-liquid membrane crystalliser where CO_2 absorbed within an NH_3 rich solution induces supersaturation through continuous CO_2 flux from the gas phase leading to nucleation of an NH_4HCO_3 product.
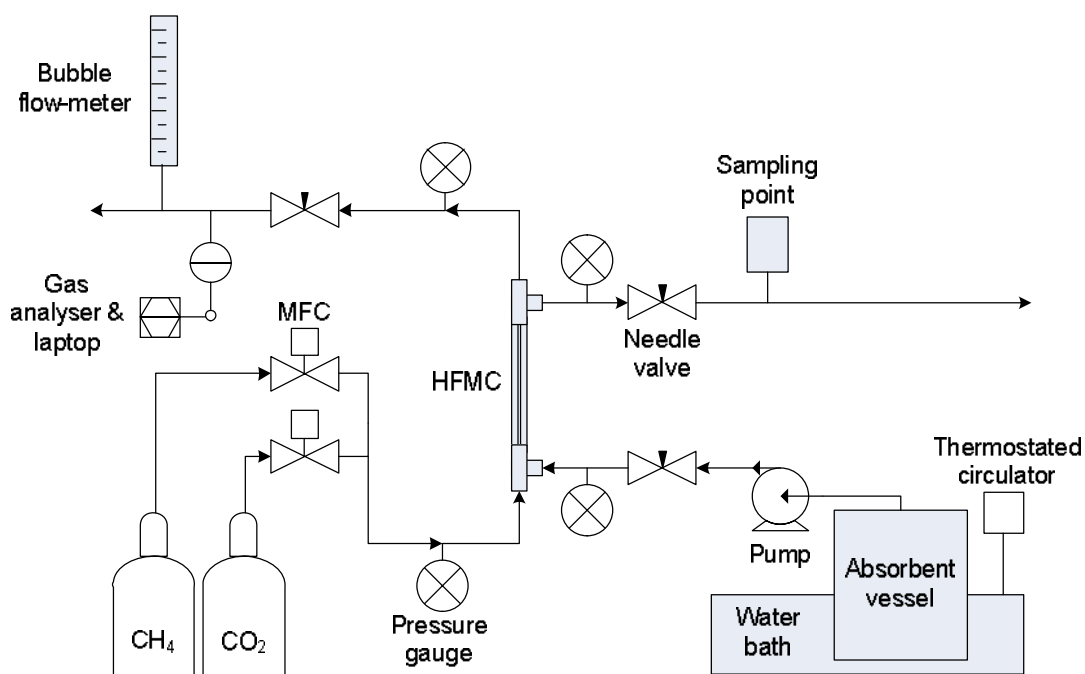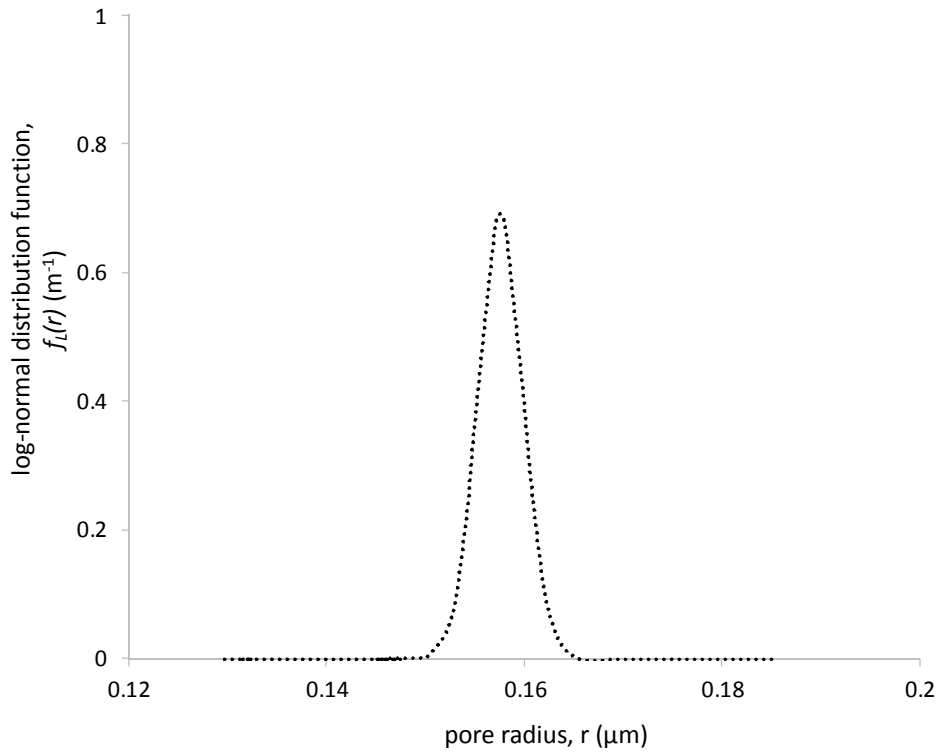

Figure 2. Schematic of experimental apparatus.

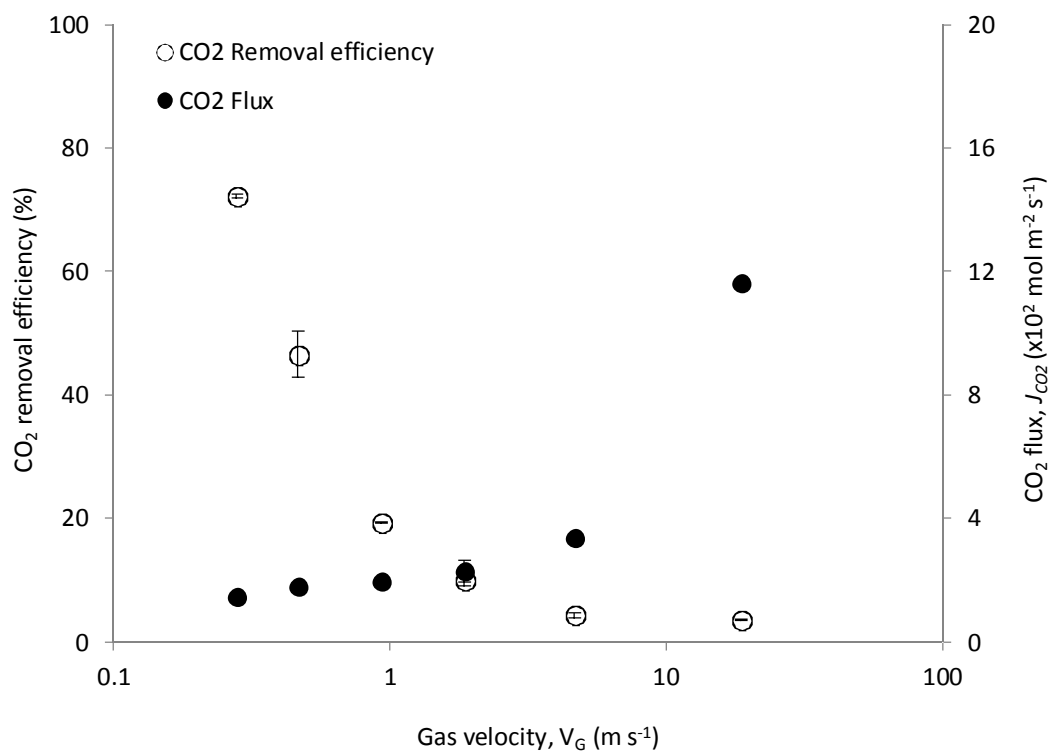Figure 3. Statistical determination of pore radii using log-normal distribution.

Figure 4. Effect of variable gas velocity (V_G) upon CO_2 removal efficiency; and CO_2 flux, during absorption from a 50:50 CO_2:CH_4 gas mixture using 7 mol l^{-1} aqueous ammonia solution at fixed liquid velocity (V_L, 0.02 m s^{-1}) in a single fibre PTFE HFMC. Error bars indicate standard error.
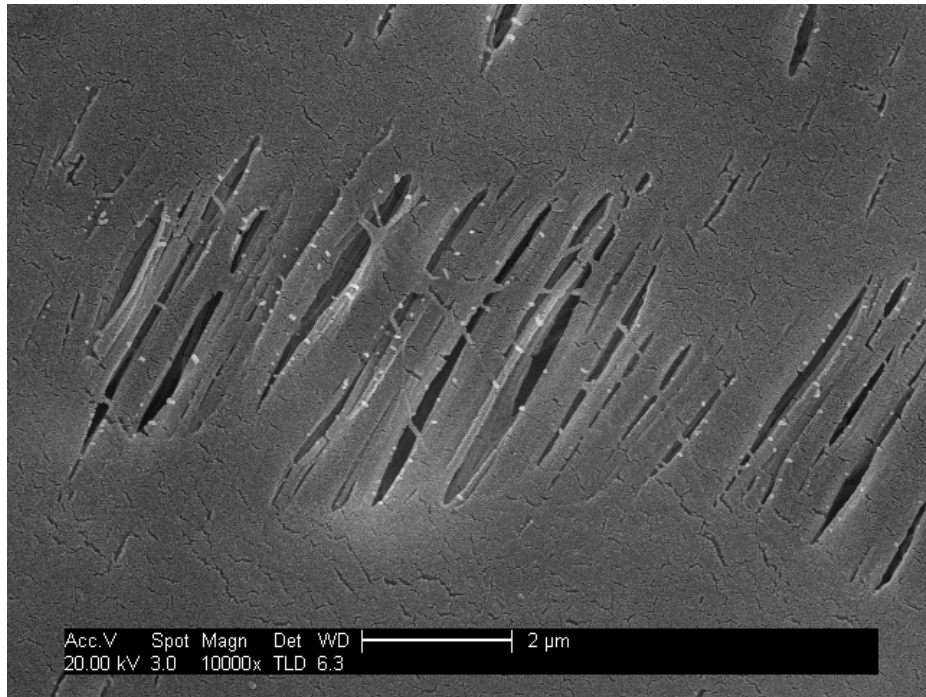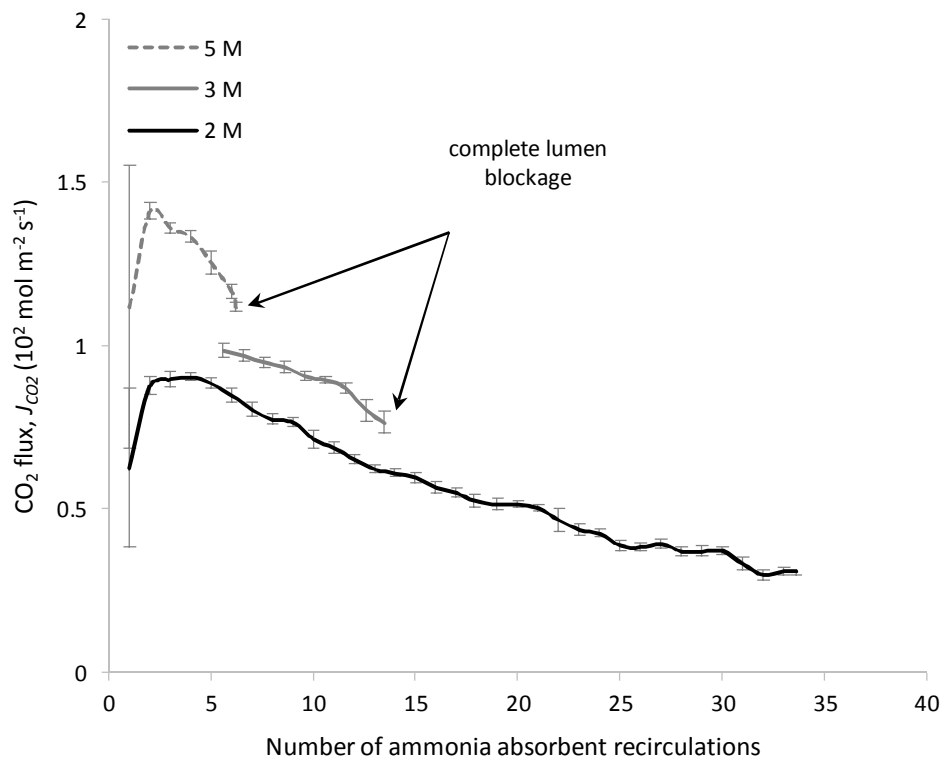
Figure 6. Carbon dioxide flux observed with the PTFE membrane following ammonia absorbent recirculation (2 M, 3 M and 5 M) through the shell-side of the module. Hydrodynamic conditions: G/L 10; V_G 0.93 m s^{-1}; V_L 0.02 m s^{-1}. Lumen side blockage observed for 3M and 5M solutions. Error bars indicate standard error.
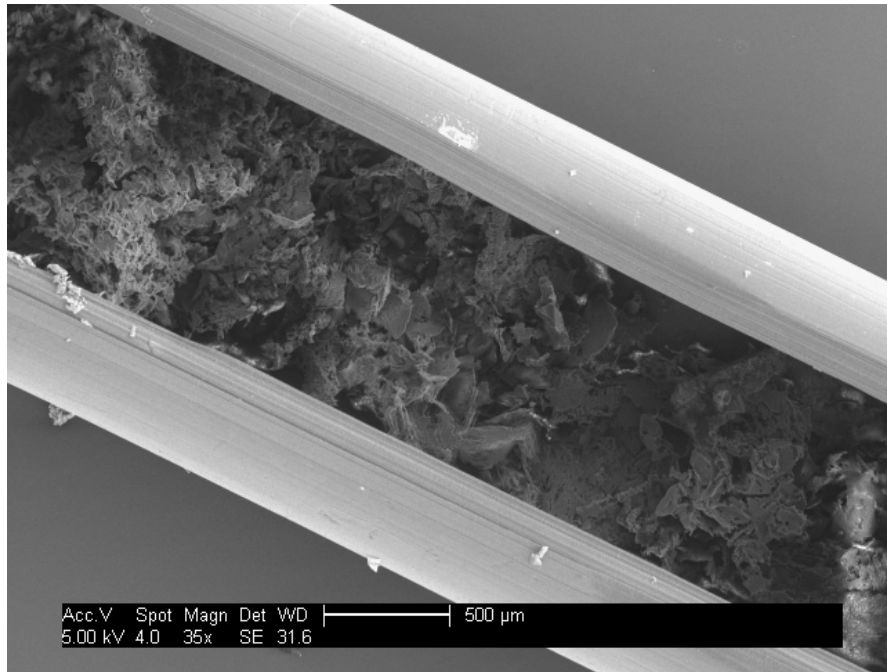
Figure 7. Dissected section of the micro-porous PTFE hollow fibre membrane used for 5M NH_3 absorbent recirculation. The experiment was stopped after 6 recirculations due to gas-side (lumen side) blockage. SEM analysis demonstrates fibre blockage due to formation of NH_4HCO_3 crystals. Hydrodynamic conditions: G/L 10; V_G 0.93 m s^{-1}; V_L 0.02 m s^{-1}.
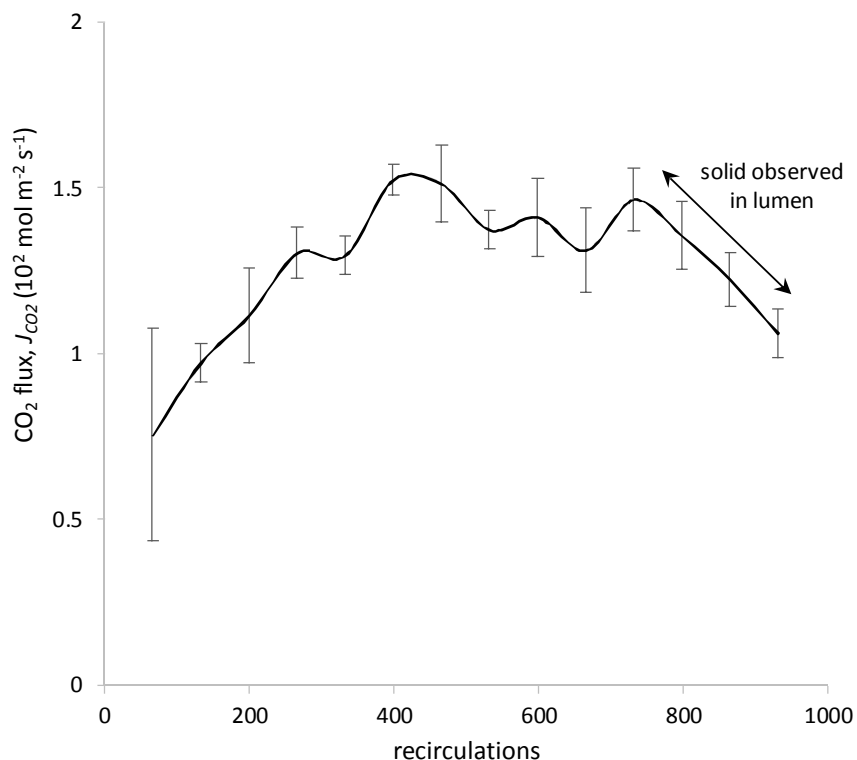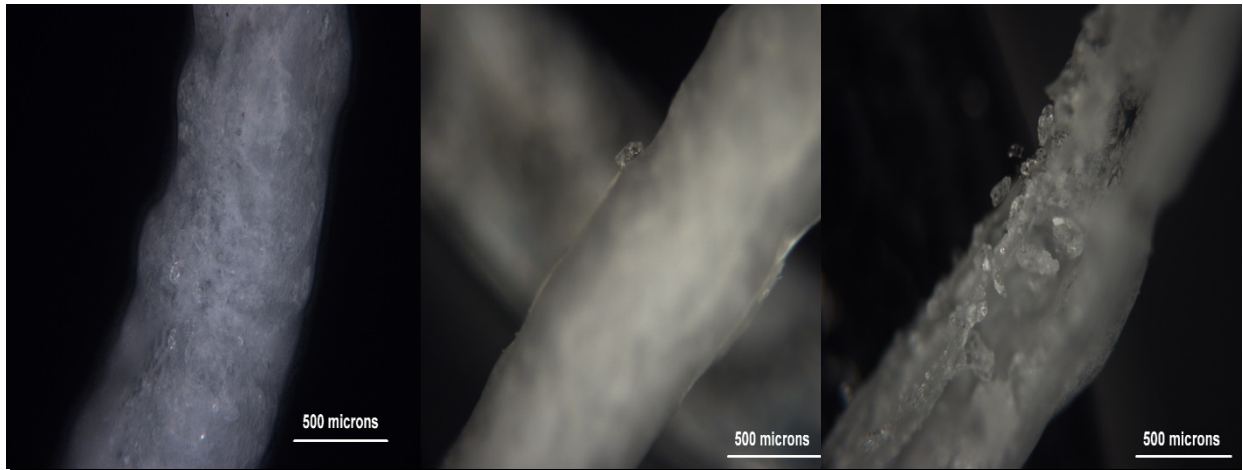

Figure 8. Carbon dioxide flux observed with the nonporous PDMS hollow fibre membrane using 5M NH_3 absorbent recirculated through the module shell-side. Gas-side (lumen side) blockage noted following 800 solvent recirculations. Hydrodynamic conditions: G/L 0.4; V_L 0.1 m s^{-1}. Error bars indicate standard error.

(a)   (b)   (c)

Figure 9. Nonporous PDMS hollow fibre membrane following >800 recirculations of 5M NH_3 absorbent: (a) crystals formed inside the fibre lumen; (b) an example crystal formed on the outside of the fibre; and (c) the PDMS fibre dissected reveals crystals formed within the fibre lumen.
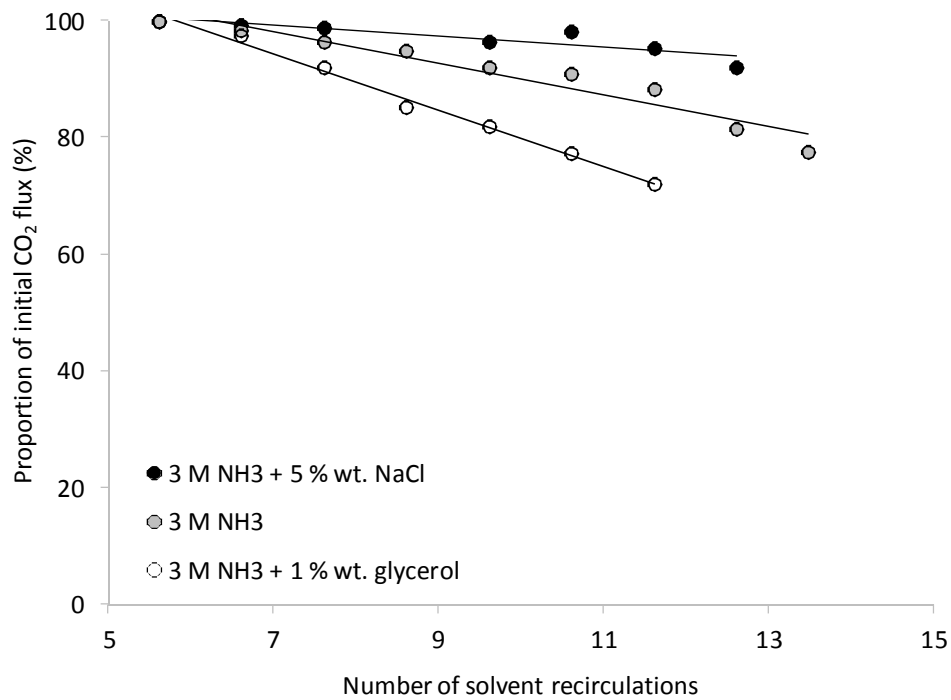
Figure 10. Impact of sodium chloride (5% NaCl) and glycerol (1% $C_3H_8O_3$) on CO_2 flux when used as additives to 3M NH_3 absorbent recirculated through the module shell-side. Hydrodynamic conditions: G/L 10; V_G 0.93 m s^{-1}; V_L 0.02 m s^{-1}.

Figure 11. Changes in surface tension relative to deionised water driven by aqueous ammonia and sodium chloride solute concentration within the concentration range examined (NH_3, 2-7M; NaCl 5% wt. or 0.85 M) (Weissenborn et al., 1995).

Figure 12. Impact of liquid-surface contact angle on the thermodynamic favourability of heterogeneous vs. homogeneous nucleation calculated for the non-porous PDMS membrane and PTFE micro-porous membrane used (Appendix, Eq. A1).
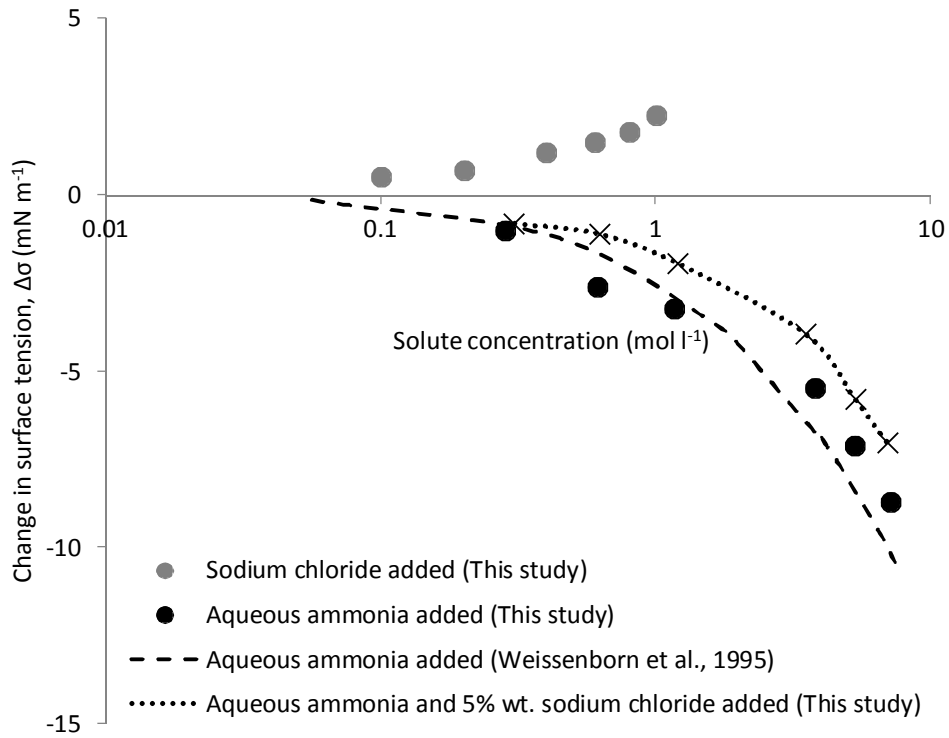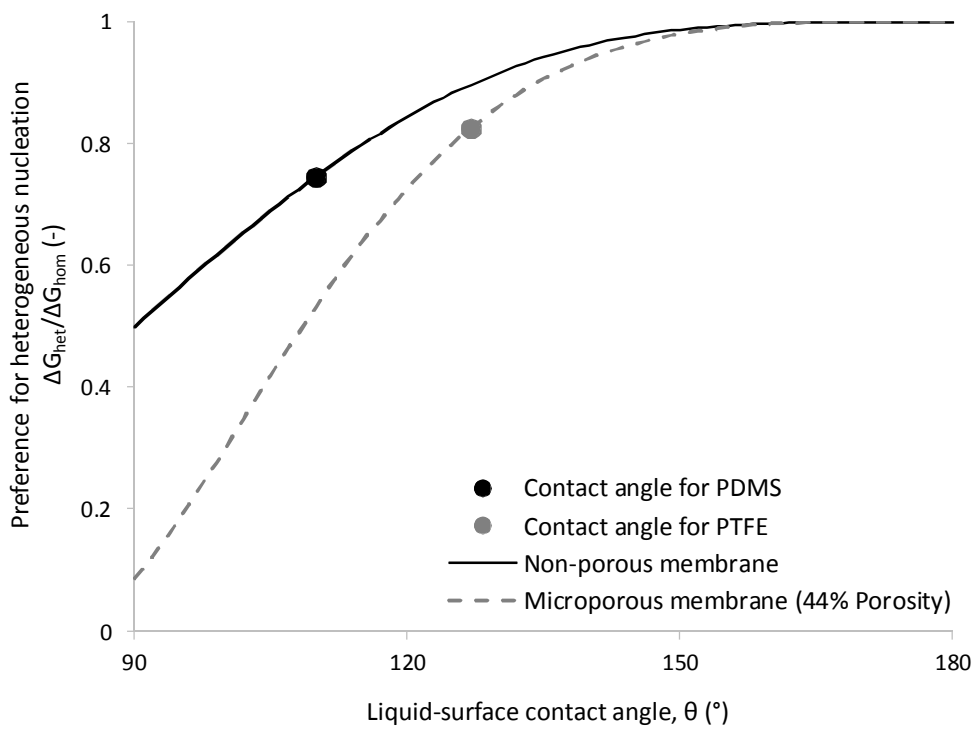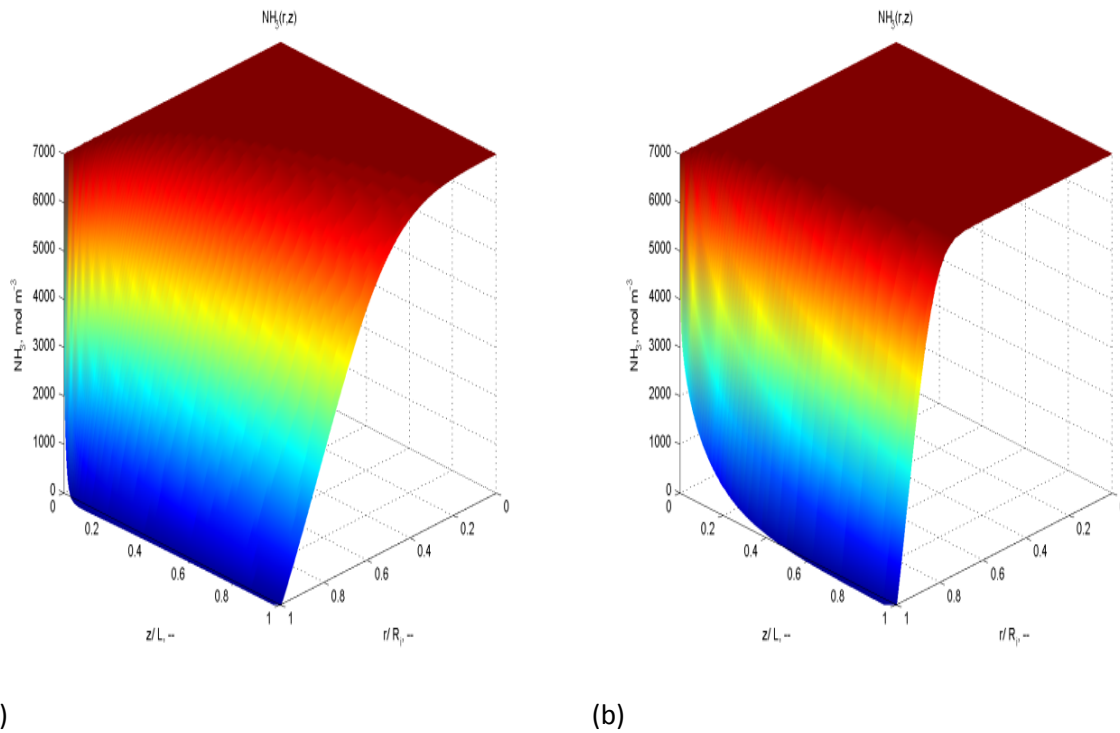

(a)   (b)

Figure 13. An illustration of NH_3 depletion by chemical reaction with CO_2: (a) extending into the liquid bulk at low V_L; and (b) confined to the liquid boundary layer at high V_L. For supporting calculations, see Appendix.

Table 1. Dimensions and surface characteristics of the single membrane fibres

		PDMS[b]	PTFE[b]
Fibre characteristics			
Inner diameter	mm	0.18	1.51
Outer diameter	mm	0.31	1.91
Wall thickness	µm	65	200
Active length	m	0.1	0.1
Surface area[a]	m^2	0.97×10^{-4}	6×10^{-4}
Porosity	%	-	44
Mean pore radius	µm	-	0.16
Average surface roughness[c]	nm	76.6	82.2
Lumen cross sectional area	m^2	2.54×10^{-8}	1.79×10^{-6}
Shell-side characteristics			
Inner diameter	mm	6	6
Outer diameter	mm	4	4
Shell cross sectional area	m^2	2.82x10-5	2.54x10-5
Priming volume	ml	2.82	2.54
Operational Characteristics			
Flow regime		Co-current	Co-current
Shell-side		5 M NH_3 (aq.)	2,3,5,7 M NH_3 (aq.)
Lumen-side		50:50 CO_2:CH_4	50:50 CO_2:CH_4

[a]Based on fibre outer diameter. [b]Data provided by manufacturer. [c]Measured using AFM.

Table 2. SEM images and EDX analyses of ammonium bicarbonate crystals grown on the PTFE membrane at the membrane-absorbent interface (shell-side) during recirculation of aqueous ammonia absorbents ranging 2 to 5 mol l^{-1} in concentration.

	2 mol l^{-1}	3 mol l^{-1}	5 mol l^{-1}
SEM/ SFEG			
EDX			

Table B1. Parameters determined for modelling of CO_2 absorption in NH_3 solutions of concentrations relevant to the present study adjusted for a system at 25 °C

c_{NH3}	x_{NH3}	$\eta^{NH3\,(aq.)}$	$D_{CO2}^{NH3\,(aq.)}$	$D_{NH3}^{NH3\,(aq.)}$	η^{H2O}	m_{CO2}	D_{CO2}^{H2O}	k_2	$k_{NH3}k_2/k_{-1}$	$k_{H2O}k_2/k_{-1}$	A_{k2}	$A_{kNH3k2/k-1}$	$A_{kH2Ok2/k-1}$
kmol m⁻³	(-)	10⁴ Pa s	10⁹ m² s⁻¹	10⁹ m² s⁻¹	10⁴ Pa s	(-)	10⁹ m² s⁻¹	m³ mol⁻¹ s⁻¹	m⁶ mol⁻² s⁻¹	m⁶ mol⁻² s⁻¹	10³ K⁻¹	10³ K⁻¹	10³ K⁻¹
2	0.038	9.61	1.80	2.11	8.84	0.83	1.92	7.5	3.8x10⁻⁴	2.6x10⁻⁶	3.0	8.5	5.5
3	0.058	9.82	1.76	2.17	"	"	"	"	"	"	"	"	"
5	0.102	10.29	1.70	2.31	"	"	"	"	"	"	"	"	"
7	0.151	10.82	1.63	2.47	"	"	"	"	"	"	"	"	"